PASJ: Publ. Astron. Soc. Japan **54**, 481–491, 2002 June 25

Relation between a Moreton Wave and an EIT Wave Observed on 1997 November 4

Shigeru ETO,[1] Hiroaki ISOBE,[2] Noriyuki NARUKAGE,[1] Ayumi ASAI,[2] Taro MORIMOTO,[2] Barbara THOMPSON,[3] Seiji YASHIRO,[3] Tongjiang WANG,[4] Reizaburo KITAI,[2] Hiroki KUROKAWA,[2] and Kazunari SHIBATA[2]

[1]*Department of Astronomy, Kyoto University, Sakyo-ku, Kyoto 606-8502*
eto@kusastro.kyoto-u.ac.jp
[2]*Kwasan and Hida Observatories, Kyoto University, Yamashina, Kyoto 607-8471*
[3]*NASA Goddard Space Flight Center, Greenbelt, MD 20771, U.S.A.*
[4]*Max-Plank-Institut für Aeronomie, Max-Plank-Str. 2, D-37191 Katlenburg-Lindau, Germany*

(Received 2002 January 15; accepted 2002 March 1)

Abstract

We consider the relationship between two flare-associated waves, a chromospheric Moreton wave and a coronal EIT wave, based on an analysis of an X-class flare event in AR 8100 on 1997 November 4. A Moreton wave was observed in Hα, H$\alpha+0.8$ Å, and H$\alpha-0.8$ Å with the Flare-Monitoring Telescope (FMT) at the Hida Observatory. An EIT wave was observed in EUV with the Extreme ultraviolet Imaging Telescope (EIT) on board SOHO. The propagation speeds of the Moreton wave and the EIT wave were approximately 715 km s^{-1} and 202 km s^{-1}, respectively. The times of visibility for the Moreton wave did not overlap those of the EIT wave, but the continuation of the former is indicated by a filament oscillation. Data on the speed and location clearly show that the Moreton wave differed physically from the EIT wave in this case. The Moreton wave preceded the EIT wave, which is inconsistent with an identification of the EIT wave with a fast-mode MHD shock.

Key words: Sun: chromosphere — Sun: corona — Sun: flares — Sun: MHD

1. Introduction

Moreton waves are flare-associated waves seen in Hα, especially in the wing of Hα (Moreton 1960, 1961; Moreton, Ramsey 1960; Athay, Moreton 1961; Smith, Harvey 1971). They propagate within a somewhat restricted solid angle at speeds of $\sim$ 400–1100 km s^{-1}. They have arclike fronts, and are often associated with type-II radio burst (Kai 1970). Uchida (1968, 1970, 1974) established that Moreton waves are a chromospheric manifestation of MHD fast-mode shocks propagating in the corona. However, the generation mechanism of Moreton waves has not yet been clarified.

Recently, the Extreme ultraviolet Imaging Telescope (EIT) aboard the Solar and Heliospheric Observatory (SOHO) discovered another wave-like phenomenon in the solar corona, which is now called EIT waves (Moses et al. 1997; Thompson et al. 1998). They are associated with flares or coronal mass ejections (CMEs), and propagate at speeds of 200–300 km s^{-1}, sometimes nearly isotropic in direction. It is also known that EIT waves are well associated with type-II radio bursts (Klassen et al. 2000). Thompson et al. (1999, 2000) suggested that EIT waves are coronal manifestation of Moreton waves. However, marked differences in the propagation pattern and speed are a big puzzle, which raises the question whether EIT waves are the same as Moreton waves.

The purpose of this paper is to examine this question based on Hα images taken with the Flare-Monitoring Telescope (FMT) at the Hida Observatory of the Moreton wave associated with an X-class flare on 1997 November 4 and the EUV images of the EIT wave taken with the SOHO/EIT of the same flare. These data show that the Moreton wave is different from the EIT wave.

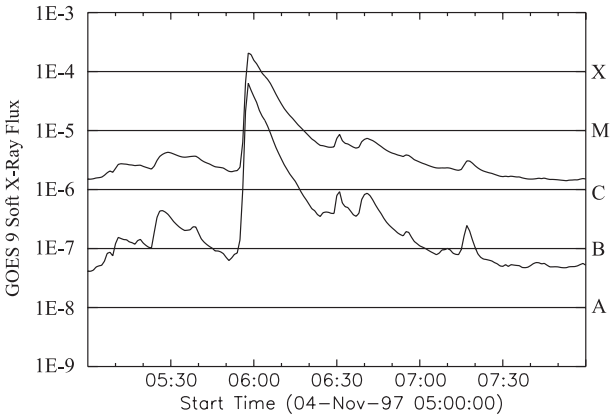

Fig. 1. X-ray emission for 05:00–08:00 UT on 1997 November 4 as recorded by GOES at the 1–8Å channel (higher flux curve) and at the 0.5–4Å channel (lower flux curve). The flare started at 05:52 UT and the time of its peak was 05:58 UT.

In section 2, the observing methods and instrumentations are summarized. In section 3, the main results of an analysis of the Moreton wave and the EIT wave are described; in section 4, a summary and a discussion are given.

2. Observations

In this paper, we consider two kinds of flare-associated waves, a chromospheric Moreton wave and a coronal EIT wave accompanied by an X-class flare, which occurred in NOAA 8100 at S14°, W34° at 05:52 UT on 1997 November 4. A GOES plot of the flare is shown in figure 1. The flare started

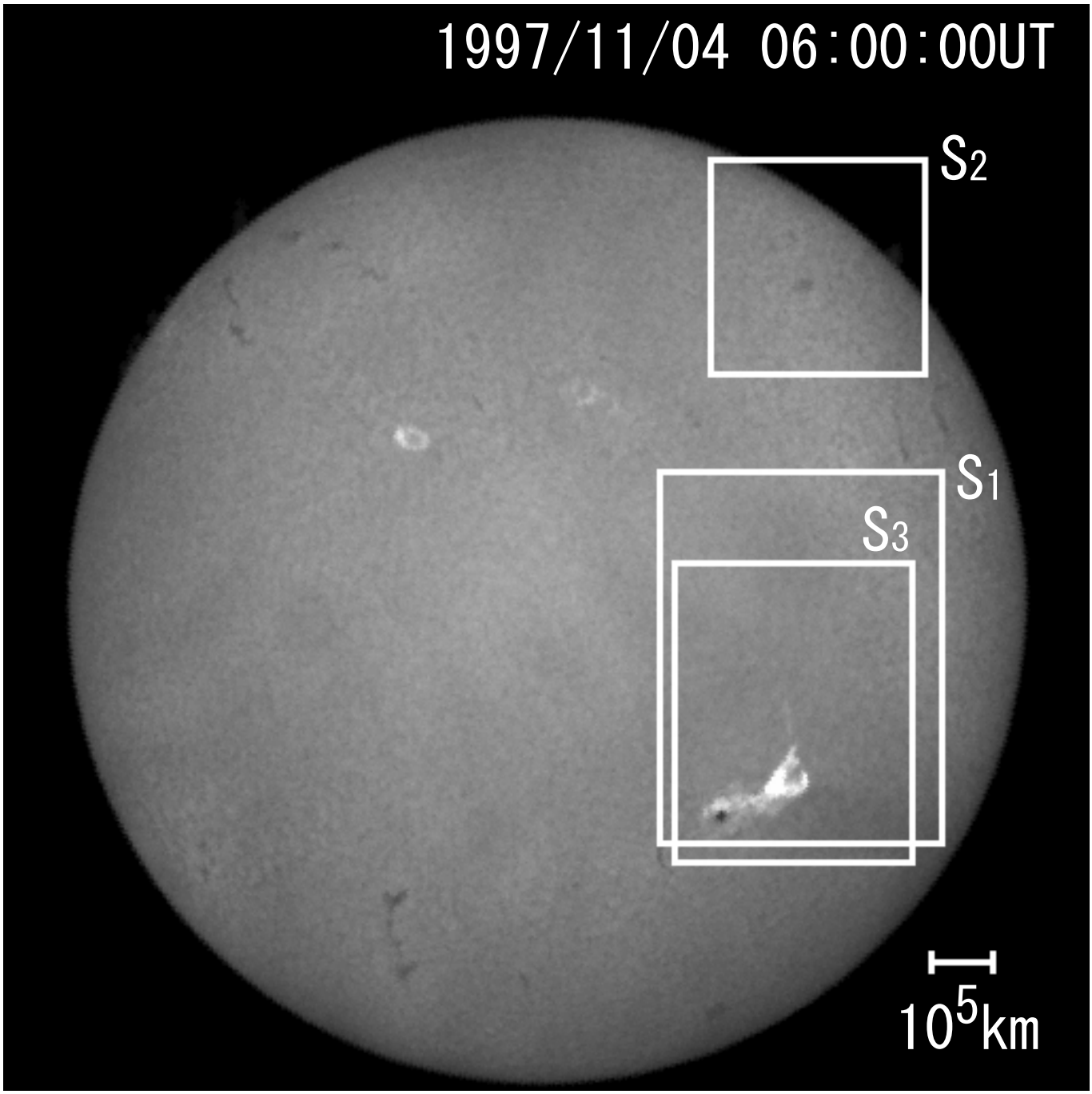

Fig. 2. Full Sun Hα (center) image at 06:00:00 UT on 1997 November 4, taken with FMT at Hida Observatory. An Hα brightening is seen in box S3, which is due to an X-class flare which started at 05:52 UT. The field of view of figures 3 and 4 is box S1. Boxes S2 and S3 correspond to the fields of view shown in figures 5 and 10, respectively.

at 05:52 UT, and its peak was at 05:58 UT. We also consider the CME, the type-II radio burst and the prominence eruption associated with the flare. Unfortunately, Yohkoh missed this event because of its night.

The Moreton wave and the prominence eruption were observed in Hα with the Flare-Monitoring Telescope (FMT) (Kurokawa et al. 1995) at the Hida Observatory of Kyoto University. The FMT observes four full disk images in Hα center, H$\alpha+0.8$ Å, H$\alpha-0.8$ Å, and continuum, and one solar limb image in Hα center. We used three full disk images in Hα center, H$\alpha+0.8$ Å, and H$\alpha-0.8$ Å. Figure 2 shows the image in Hα center at 6:00:00 UT. The flare occurred in the bright region in the southwest. The time resolution of the Hα images used in this paper is 1 min, though the FMT operates at a higher time resolution. The exact times of Hα center, H$\alpha+0.8$ Å, and H$\alpha-0.8$ Å were 0 s, 1 s, and 2 s after each minute during the

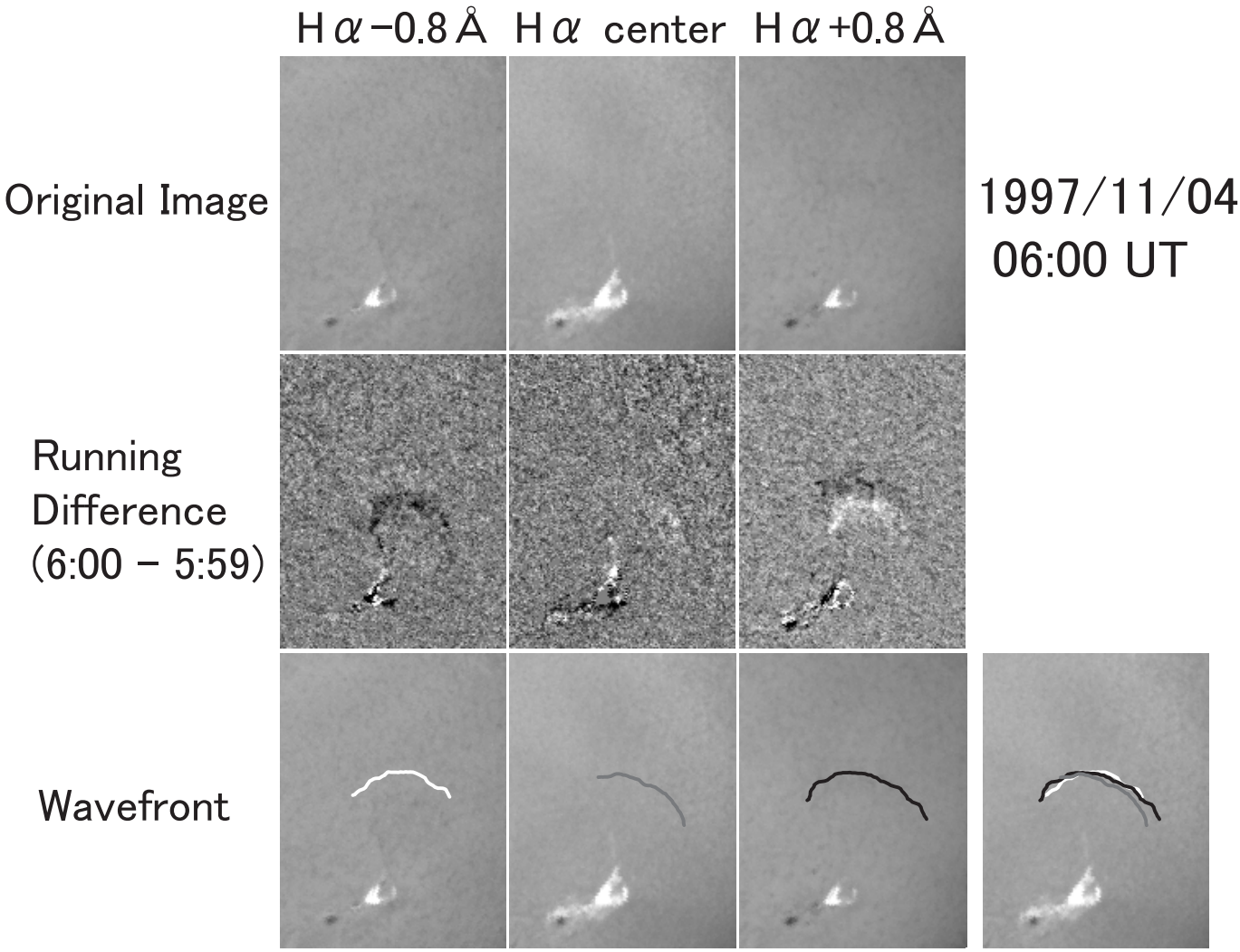

Fig. 3. Locations of the Moreton wave in H$\alpha - 0.8$ Å (left), Hα center (center), and H$\alpha + 0.8$Å (right) at 06:00 UT on 1997 November 4. The field is box S1 in figure 2. The top panels are original images. The middle panels are the "Running difference" images which are images at 06:00 UT subtracted by a previous image at 05:59 UT. The bottom panels show the location of the Moreton wave identified with each wavelength image. The wave fronts of H$\alpha - 0.8$ Å, Hα center, and H$\alpha + 0.8$Å images are shown by the white, gray, and black curves, respectively. The right image shows the wave-fronts at all wavelengths.

observed time interval. These differences in the observed times were negligible in this study, because a wave with a velocity of 1000 km s^{-1} propagates 2000 km in 2 s, and this distance is within the pixel scale. The velocity of the wave which we will discuss was less than 1000 km s^{-1}.

The EUV images were observed with the EIT (Delaboudinière et al. 1995) on board SOHO. The observation in the present study consisted of a wavelength range centered on 195 Å, comprising a Fe XII line emitted at 1.2×10^6 K at typical coronal density. The time resolution was about 17 min.

A CME was observed with the Large Angle and Spectrometric Coronagraph (LASCO, Brueckner et al. 1995) on board SOHO. A type-II radio burst was recorded with the Hiraiso Radio Spectrograph (HiRAS, Kondo et al. 1995).

3. Results

Figure 3 shows the FMT images observed in H$\alpha - 0.8$ Å (left column), Hα center (middle column), and H$\alpha + 0.8$ Å (right column) in box S1 indicated in figure 2. The top panels show the original images at 06:00 UT, and the middle panels show "running difference" images, or the images at 06:00 UT, which were subtracted by a previous image at 05:59 UT. In the running difference images the wave-fronts of the Moreton wave can be clearly seen. In the bottom panels the wave-fronts identified in the running difference image in each wavelength are overlaid on the original images. The white, gray, and black lines illustrate the wave-fronts in H$\alpha - 0.8$ Å, Hα center, and H$\alpha + 0.8$ Å, respectively. As shown in the right-bottom panel, the locations of the wave-fronts are not much different in the three wavelengths images. Thus, in the following analyses we use H$\alpha + 0.8$Å images, in which the wave-fronts are most

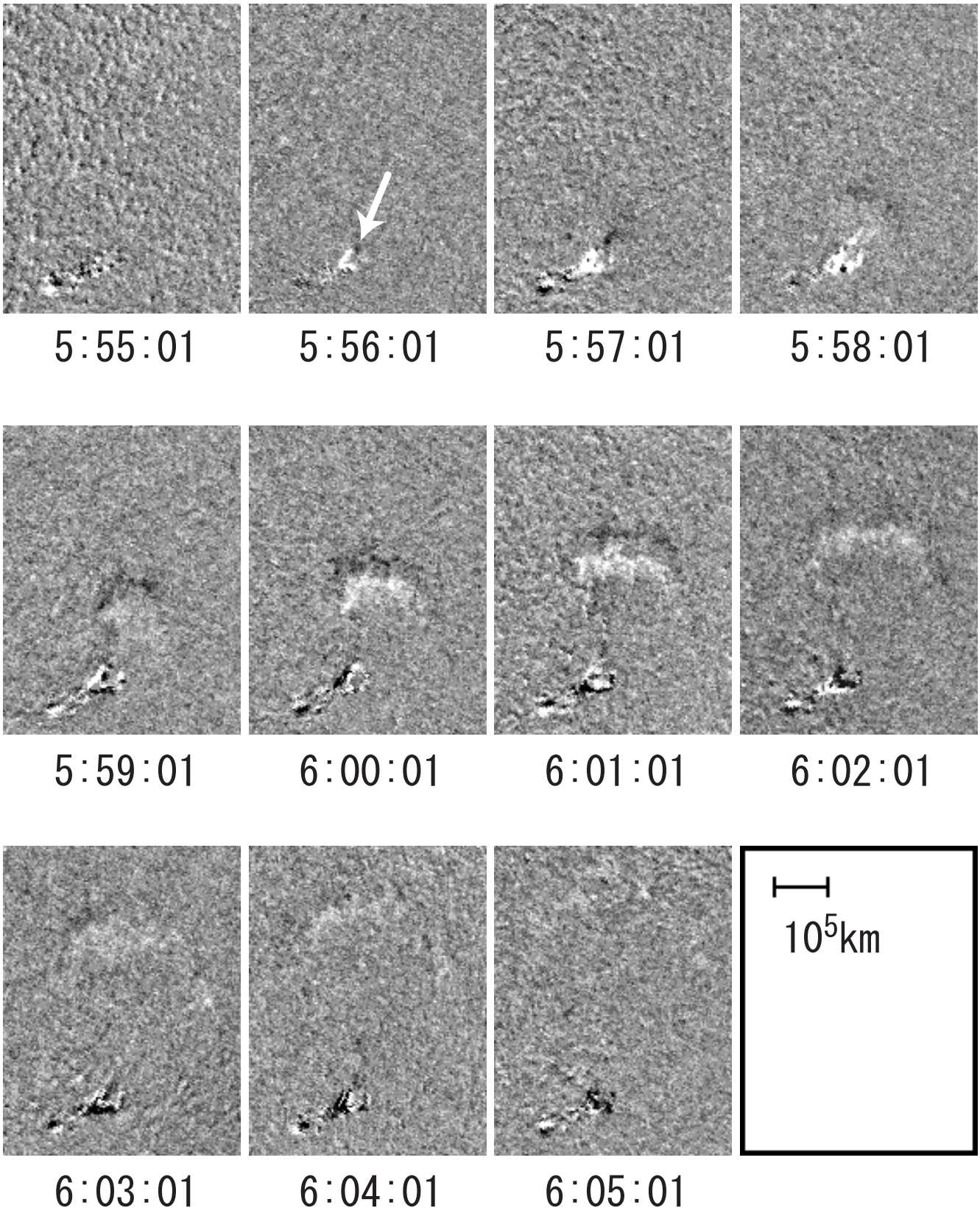

Fig. 4. Running differences of Hα + 0.8Å images taken at every minute from 05:57:01 UT to 06:08:01 UT. The field of view is box S1 in figure 2. The wave-fronts of Moreton wave can be clearly seen as dark and white strips.

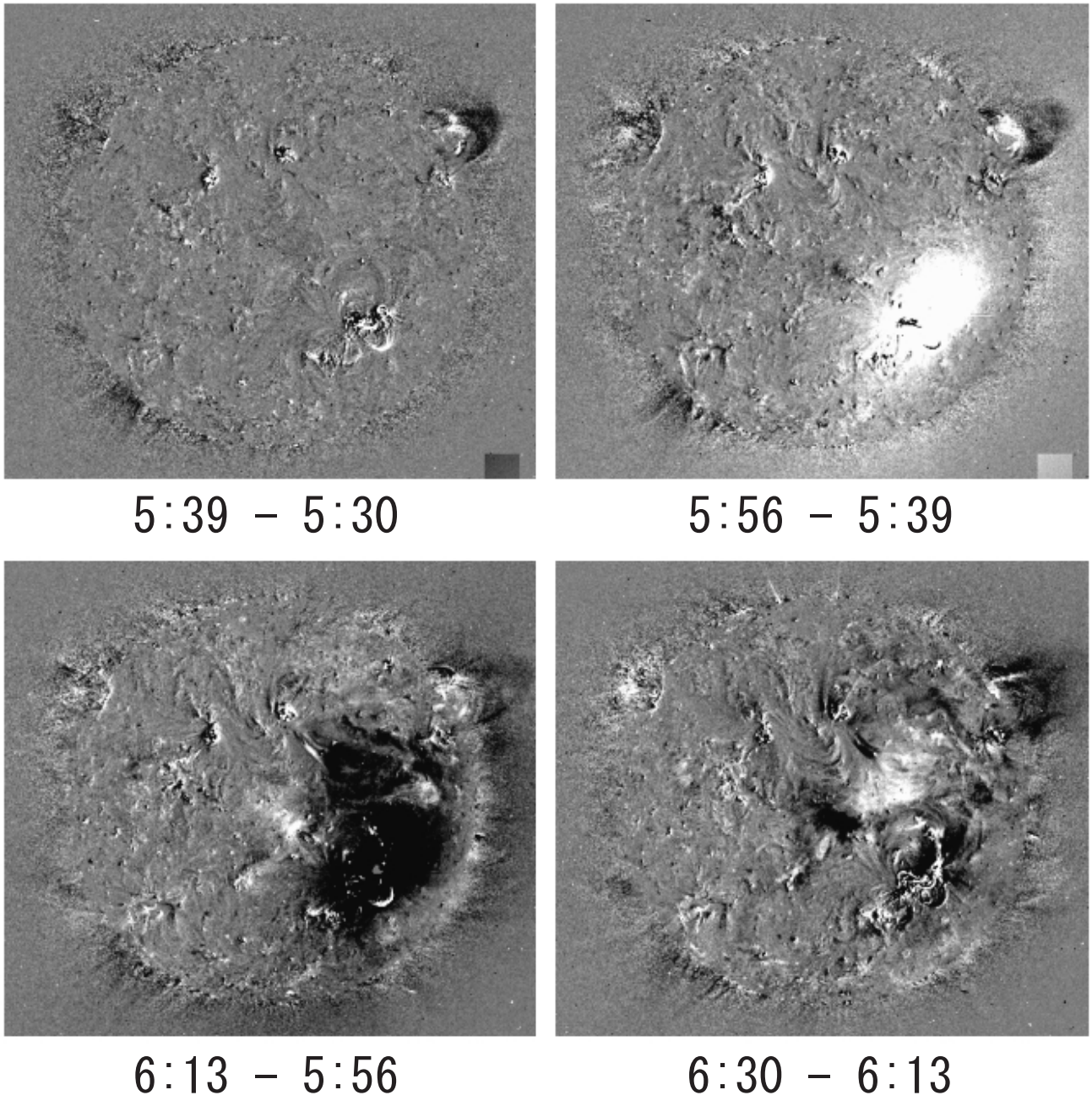

Fig. 5. Running differences of EIT images. The top-left panel shows the image at 05:39 UT subtracted by that of 05:30 UT, and so on. The white oval region in the top-right panel is mainly due to scattered light in the telescope. In the lower panels the disturbance seems to propagate away from the flare site.

clearly seen.

The running difference images of Hα + 0.8Å are shown in figure 4. The field of view is illustrated by box S1 in figure 2. The dark small region indicated by the arrow in the image at 05:56:01 UT in figure 4 seems to be an origination point of the Moreton wave. It is different from the brightest region during the flare at Hα, which is the white region in the image at 05:57:01 UT in figure 4. We define the brightest region as a flare site. The wave-fronts of the Moreton wave can be identified in the images from 05:58 UT to 06:04 UT. In the images after 06:05 UT, the Moreton wave is too diffuse to identify its wave-front. Naturally, this does not mean that the Moreton wave stopped propagating at 06:04 UT. It probably propagated farther after 06:04 UT, though its wave-front can not be seen. As reported later, there is indirect evidence that the Moreton wave propagated farther near the northwest limb, though its wave-front is not seen in the region.

Figure 5 shows the running differences of the EIT images.

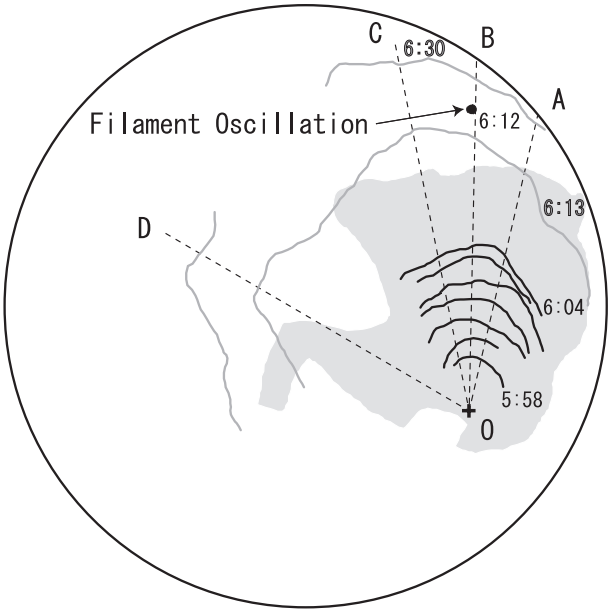

Fig. 6. Observed wave-fronts of the EIT wave (gray lines) and the Moreton wave (black lines), and the dimming region (light gray region). The EIT wave-fronts are those at 06:13 UT and 06:30 UT, and the Moreton wave-fronts are those from 05:58:01 UT to 06:04:01 UT with interval of 1 min. The location of the filament which started to oscillate from about 06:12:00 UT is also indicated by the black filled circle. The dimming region corresponds to the dark region in a running difference image at 6:13–5:56 UT in figure 5, which is a depletion region during this period. The distances of wave-fronts from the flare site **O** along the lines **O–A**, **O–B**, **O–C**, and **O–D** are plotted in figure 7.

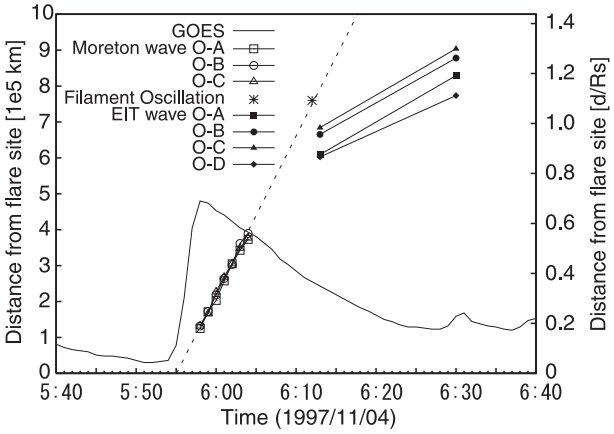

Fig. 7. Time evolutions of the distance of the Moreton wave (open symbols) and the EIT wave (filled symbols) from the flare site (point **O** in figure 6) along the lines **O–A**, **O–B**, **O–C**, and **O–D** in figure 6. An asterisk at 06:12:00 UT represents the start of the filament oscillation and the distance of the filament from the flare site. To illustrate the flare start and its peak, GOES X-ray flux data at the 1–8Å channel (higher flux curve in figure 1) are overplotted. 'Rs' represents the solar radius (695800 km).

A disturbance is seen to propagate from the flare site. The bright oval structure in the 05:56 UT image (upper-right panel) is mainly due to scattered light in the telescope, and is probably not a real wave-front. Hence, the wave-fronts in the EIT images are identified only at 06:13 UT and 06:30 UT. On the other hand, the wave-fronts of the Moreton wave are identified from 05:58 UT to 06:04 UT. Thus, we can not directly compare the locations of the Moreton wave and the EIT wave at the same time.

Figure 6 shows the wave-fronts of the Moreton wave (black lines) from 05:58:01 UT to 06:04:01 UT every minute, those of the EIT wave (gray lines) at 06:13 UT and 06:30 UT, and the coronal dimming region observed in the EIT images. Point **O** indicates the flare site. Although both the EIT wave and the Moreton wave propagate northward, the angles of their propagation are different. While the Moreton propagates in a narrow angle of about 60°, the EIT wave propagates in a

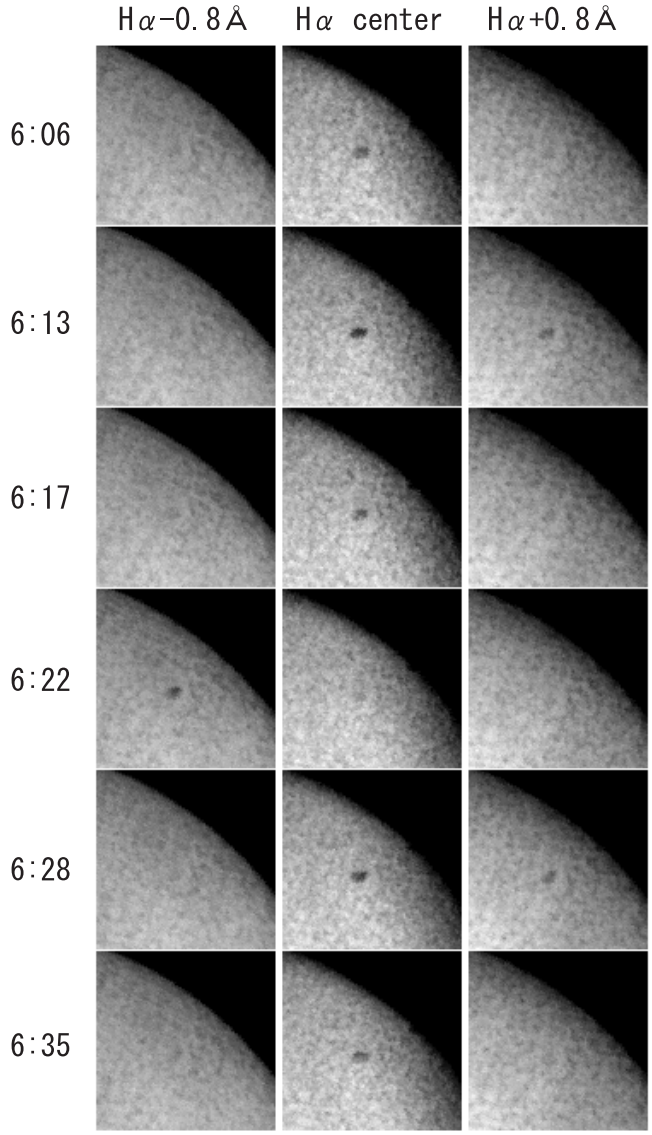

Fig. 8. Hα images (Hα − 0.8 Å; left, Hα center; center, and Hα + 0.8 Å; right) of an oscillating dark filament. The field of view is box S2 in figure 2. The filament started to oscillate at about 06:12:00 UT. The faint dark filament was seen in the Hα + 0.8Å at 06:13 UT, which means that the filament was undergoing downward motion, whereas the filament disappeared in the Hα center and appeared in the Hα − 0.8 Å image at 06:22 UT, indicating that the filament was undergoing upward motion at 06:22 UT.

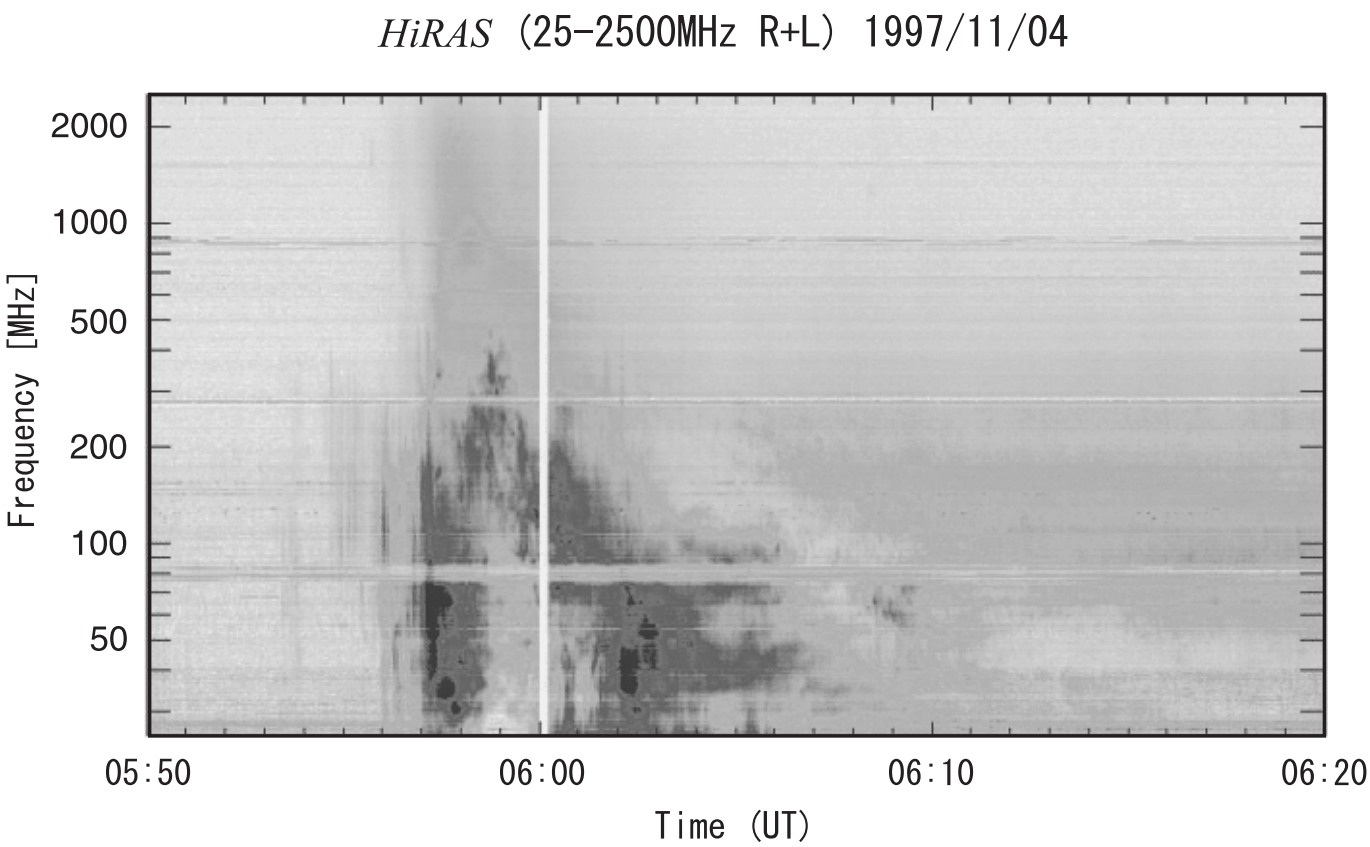

Fig. 9. Metric radio data for 05:50–06:20 UT on 1997 November 4 observed with the Hiraiso Radio Spectrograph (HiRAS), showing type-II and type-III radio bursts. The almost vertical line at about 05:58 UT represents the type-III radio burst, and the burst about from 05:59 UT to 06:06 UT is the type-II radio burst.

relatively wide angle. The distances of the wave-fronts from the flare site **O** along the lines **O–A**, **O–B**, **O–C**, and **O–D** are plotted in figure 7. The distances are measured along the photosphere. The curvature of the solar surface is taken into account. The propagation velocity of the Moreton wave is almost constant at $715\,\mathrm{km\,s^{-1}}$. The velocities of the EIT wave are slightly different in different directions. The average velocity is $202\,\mathrm{km\,s^{-1}}$. These propagation velocities and angles are typical for both Moreton waves and EIT waves.

The FMT observed an oscillation of a quiescent filament, which is the indirect evidence mentioned above that the Moreton wave probably propagated farther after 06:04 UT. The filament is located near the northwest limb, which is indicated by the filled circle in figure 6. Figure 8 shows the FMT images of the oscillating filament at the wavelengths of H$\alpha - 0.8$ Å, Hα center, and H$\alpha + 0.8$Å. The field of view is shown by box S2 in figure 2. The oscillation of the filament started at 06:12:00 UT. We plot an asterisk in figure 7 corresponding to the starting time of the oscillation and the distance from the flare site of the filament. The asterisk almost lies on the extrapolated line of the Moreton wave. It is thus reasonable to conjecture that the filament oscillation was caused by an 'invisible' Moreton wave (Smith, Harvey 1971). If this interpretation is correct, the Moreton wave must have reached the filament near the northwest limb at 06:12:00 UT. On the other hand, the EIT wave did not reach the filament even at 06:13 UT. Consequently, we can say that the Moreton wave and the EIT wave are not co-spatial.

4. Discussion

We first discuss the identification of two flare-waves, a chromospheric Moreton wave and a coronal EIT wave. In Uchida's model (1968, 1970), which is most widely accepted, the Moreton wave is a sweeping skirt on the chromosphere of the MHD fast-mode shock which propagates in the corona. Therefore, this model predicts the existence of a coronal counterpart of the chromospheric Moreton wave at the same place and with the same velocity as that of the Moreton wave. Thompson et al. (2000) reported that there are two components in EIT waves, i.e. bright and sharp, and 'traditional' diffuse EIT waves. The sharp EIT wave and Hα Moreton wave are co-spatial, whereas the relationship between the diffuse EIT and Moreton wave was not clear. In the event discussed in this paper, only the diffuse EIT wave was observed. From similar observations reported by Thompson et al. (2000), Warmuth et al. (2001) suggested that the diffuse EIT waves are decelerated Moreton wave, namely that not only the sharp EIT waves but also the diffuse EIT waves are coronal counterparts of the chromospheric Moreton waves. In the previous section, however,

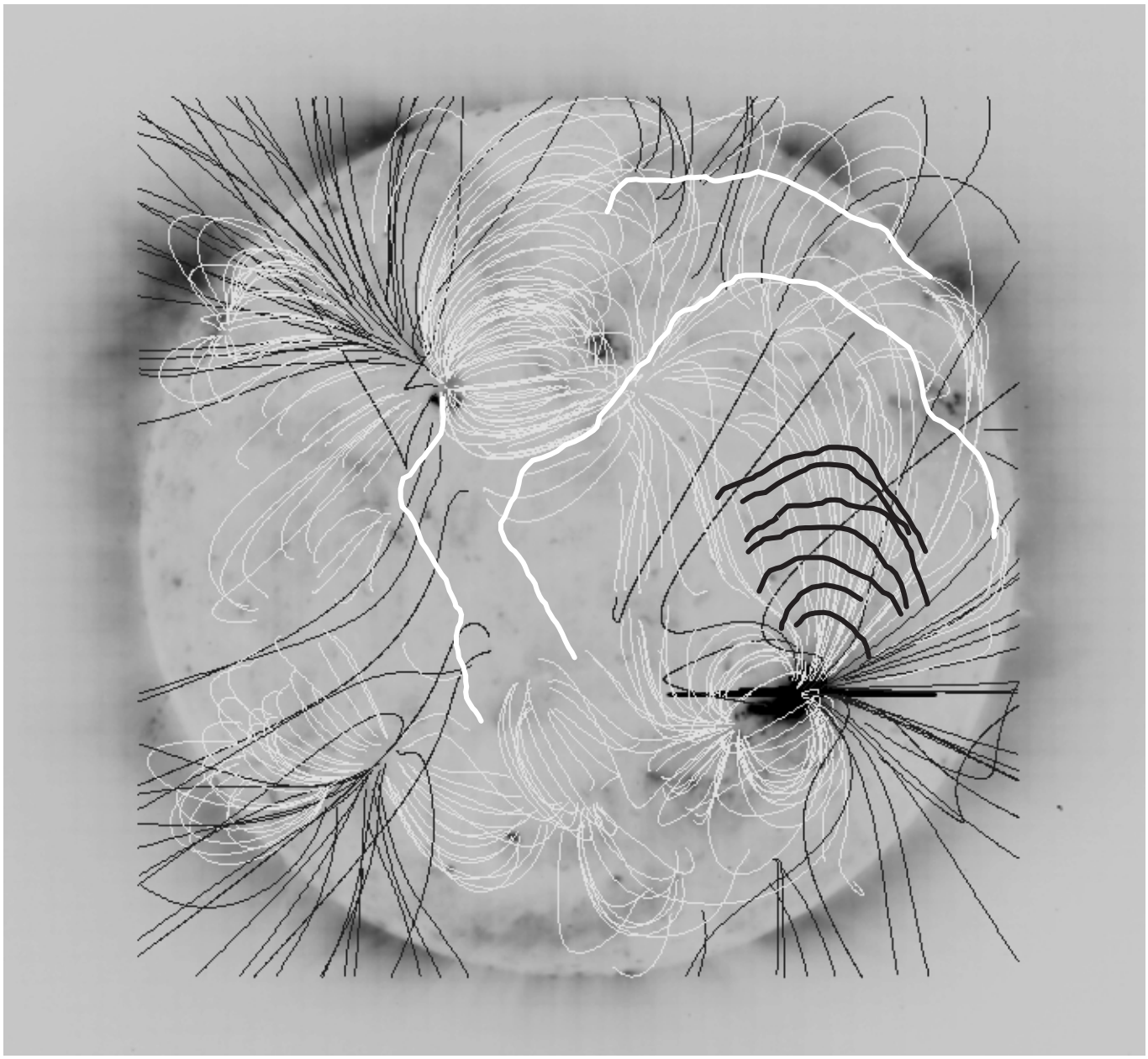

Fig. 10. Wave fronts of the Moreton wave (thick black lines) and the EIT wave (thick white lines) overlaid on the potential magnetic field lines. The thin black and white lines show the open and closed field lines, respectively. The wave fronts are the same as that in figure 6. The background is the EIT image at 05:56 UT.

we revealed that the Moreton wave and the diffuse EIT wave are not co-spatial and that they have very different velocities. Therefore, we conclude that at least in this event, the diffuse EIT wave is not the coronal counterpart of the Moreton wave.

It is worth noting that this observed fact does not deny Uchida's model. It only suggests that an EIT wave is not the coronal disturbance predicted by Uchida's model. Uchida argues that one of the conditions that Moreton wave occurs is that the flare (the source of the MHD fast-mode shock) occurs near the edge of the active region, and the direction of propagation is opposite to the active region. The event reported in this paper satisfies these conditions. The type-II burst observations, which we now discuss, are also in accordance with Uchida's model.

As mentioned above, a type-II radio burst was associated with this event. Figure 9 shows a radio spectrograph taken with HiRAS. An almost vertical line at about 05:58 UT and a curve from about 05:59 UT to 06:06 UT in figure 9 are type-III and II radio bursts, respectively. Based on the coronal electron density model (Mann et al. 1999), we can calculate the distance from the photosphere and the velocity of the type-II radio burst. The average velocity of the type-II radio burst is

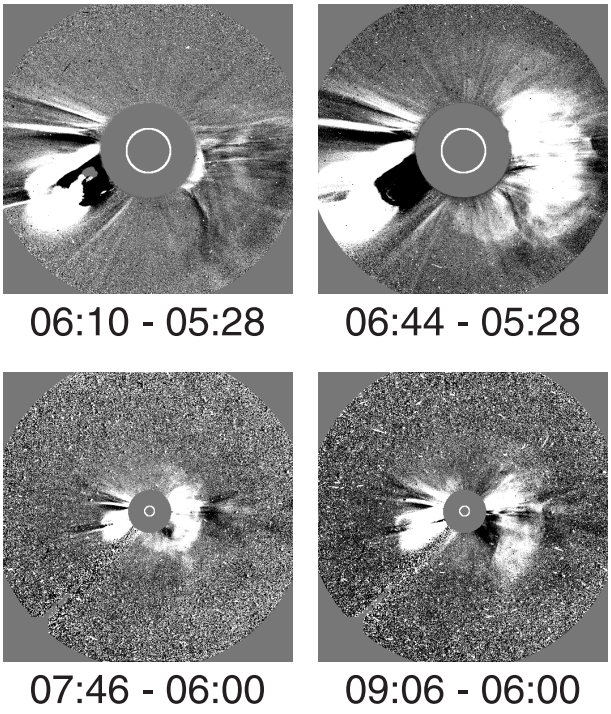

Fig. 11. SOHO/LASCO difference images showing the halo CME associated with the Moreton wave on 1997 November 4. The white circle represents the optical disk of the Sun. The upper and lower panels are C2 and C3 images, respectively. The average velocity of the leading edge is about 790 km s^{-1}.

about 890 km s^{-1}, which is close to that of the Moreton wave (about 715 km s^{-1}) compared with that of the EIT wave (about 202 km s^{-1}). Furthermore, the distances of the type-II radio burst are very similar to those of the Moreton wave, as shown in figure 13. Uchida (1974) suggests that the Moreton wave and the type-II radio burst are two aspects of one agent, or the MHD fast-mode shock propagating in the corona. The similarity of the velocity and the distances of the Moreton wave and the type-II radio burst supports this idea.

Next, we consider the relationship between the coronal magnetic field, the Moreton wave, and the EIT wave. Figure 10 shows the extrapolated coronal magnetic-field lines based on the potential field calculation (Yan et al. 1991, 1993; Wang et al. 2002) using a photospheric magnetogram obtained with the SOHO/MDI (Scherrer et al. 1995) and the wave-fronts of the Moreton wave and the EIT wave. The direction of propagation and the angular range of the wave front of the Moreton wave, at first sight, seem to be guided by the loops connected to the northern edge of the flare site where the coronal dimming was observed in the EIT images, though the filament oscillation suggests that the Moreton wave propagates across the closed magnetic loops. The visibility of the Moreton wave may be related to the magnetic field configuration and coronal dimming. On the other hand, the direction of propagation of the EIT wave dose not seem to be confined by the loops, and the EIT wave is observed outside them, namely outside the dimming region. Considering that the waves propagated across the closed magnetic field, the Moreton wave around the filament may be similar to the EIT wave. However, as we have mentioned above,

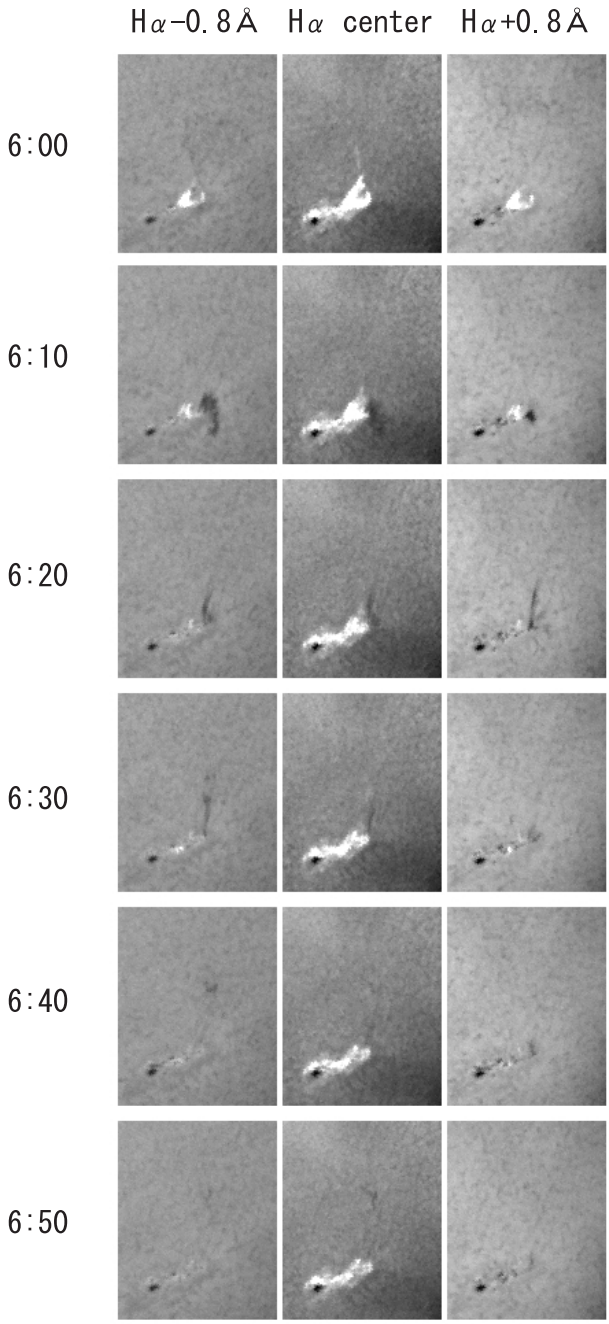

Fig. 12. Images of the prominence eruption starting from 06:00 UT on 1997 November 4 obtained in H$\alpha - 0.8$ Å (left), Hα (center), and H$\alpha + 0.8$Å (right) with FMT. The field of view is box S3 in figure 2.

the EIT wave-front is not co-spatial with the Moreton wave front suggested by the filament oscillation and the propagation speeds of both waves are clearly different. It may be possible that the Moreton wave is a super-Alfvenic shock (Wang 2000) whose propagation speed is larger than that of the MHD fast-mode wave, whereas the EIT wave is a usual fast-mode MHD wave which is excited by the Moreton wave. An alternative possibility is that the EIT wave is a trapped MHD wave with a long wavelength, whose horizontal group-velocity is much less than the fast-mode speed (Uchida et al. 2001).

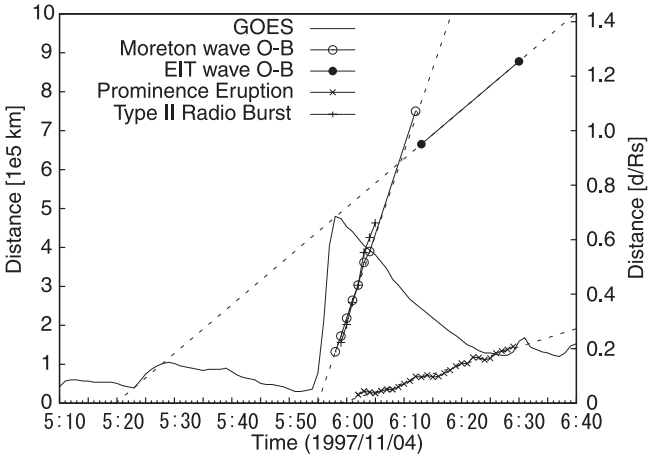

Fig. 13. Time evolutions of the distances of the Moreton wave, the EIT wave, the type-II radio burst, and the prominence eruption with GOES X-ray flux data at the 1–8Å channel (higher flux curve in figure 1). The vertical axis represents the distances from the flare site along the line **O–B** in figure 6 for the Moreton wave and the EIT wave, the distance from the photosphere calculated with the coronal electron density model for the type-II radio burst, and the projected distance for the prominence eruption. The dashed lines are extrapolated lines for the Moreton wave, the EIT wave, and the prominence eruption. 'Rs' represents the solar radius (695800 km).

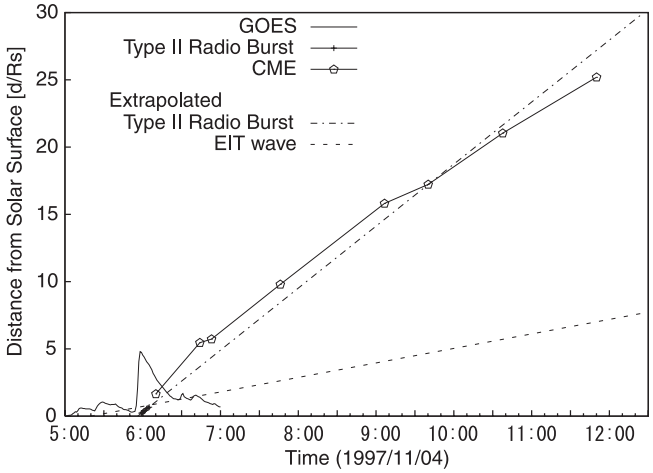

Fig. 14. Time evolutions of the distance from the photosphere of the type-II radio burst and the CME with GOES soft X-ray data at the 1–8Å channel (higher flux curve in figure 1). The distance of the type-II radio burst was calculated using the coronal electron density model. The distance of the CME was measured at a position angle of 243°. Two kinds of dashed lines represent the extrapolated lines of the type-II radio burst and the EIT wave, respectively. 'Rs' represents the solar radius (695800 km).

A halo CME was observed in association with this event. Figure 11 shows SOHO/LASCO difference images with a suitable base image in the pre-event stage subtracted. A bright leading edge appeared above the western occulting disk of the C2 coronagraph at 06:10 UT, and faint extensions surrounded the occulting disk in the second image at 06:44 UT. The average velocity of the leading edge is about 790 km s^{-1}. This velocity is again similar to that of the Moreton wave.

A prominence eruption also occurred in association with the same event. Figure 12 shows the prominence eruption at the wavelengths of H$\alpha - 0.8$ Å, Hα center, H$\alpha + 0.8$ Å at 06:00 UT, 06:10 UT, 06:20 UT, 06:30 UT, 06:40 UT, and 06:50 UT. The projected erupting velocity is about 77 km s^{-1}. The original site of the erupting prominence is different from the small black region indicated by the arrow in figure 4. The direction of the eruption is approximately the same as the direction of propagation of the Moreton wave.

Finally, we discuss the relationship between all phenomena in this event: flare, Moreton wave (including filament oscillation), EIT wave, type-II radio burst, CME, and prominence eruption. Figure 13 shows the time evolutions of the distances of the Moreton wave, the EIT wave, the type-II radio burst, and the prominence eruption with GOES X-ray flux data at the 1–8Å channel (higher flux curve in figure 1). We plot the distances from the flare site along line **O–B** in figure 6 for the Moreton wave and the EIT wave, the distance from the photosphere calculated with the coronal electron density model for the type-II radio burst, and the projected distance for the prominence eruption. The dashed lines are extrapolated lines for the Moreton wave, the EIT wave, and the prominence eruption. The rapid increase in the soft X-ray flux started at 05:55 UT, though the flare started at 05:52 UT. The extrapolated start time of the Moreton wave, the EIT wave, and the prominence eruption are 05:55 UT, 05:20 UT (estimated with all lines' data in figure 6), and 05:59 UT, respectively. As discussed above, the distance of the Moreton wave was similar to that of the type-II radio burst. The start times of the Moreton wave and the type-II radio burst were similar to that of the rapid increase in the soft X-ray flux, and the start time of the prominence eruption was nearly simultaneous with the flare peak time. These phenomena seem to be closely related to the flare. If the EIT wave actually started at 05:20 UT and propagated with a constant velocity, the disturbance should be seen in the images at even 05:30 UT and 05:39 UT. However, there is no disturbance in the running difference image at 05:39 UT subtracted by the image at 05:30 UT (upper-left panel in figure 5). This characteristic of EIT waves is also reported by Thompson et al. (1999). They suggest that the diffuse EIT waves may have started not from the flare site, but from the boundary of the coronal dimming region, since they were observed only outside the dimming region. This is also true in this event (see figure 6). It is interesting to note that the drastic change in the brightness of the oscillating dark filament in Hα center occurred at about 6:22 UT (see figure 8), which corresponds to the time when the EIT wave passed the filament.

Figure 14 shows the time evolutions of the distances from the photosphere of the type-II radio burst and the CME with GOES soft X-ray data at the 1–8Å channel (higher flux curve in figure 1). The distance of the CME was measured at a position angle of 243°. The CME seems to follow the type-II radio burst, implying a common origin. In contrast with the EIT wave, the Moreton wave, the type-II radio burst, and the CME have similar velocities. From figures 13 and 14, we can say that these phenomena, except for the EIT wave, seem to be closely involved. The relationship between these phenomena will be discussed in more detail in our future paper.

The authors wish to thank H. S. Hudson and M. Kadota for their useful comments, and the Hiraiso Solar Terrestrial Research Center for providing us with the data of the type-II radio burst. SOHO is a mission of international cooperation between European Space Agency (ESA) and National Aeronautics and Space Administration (NASA). This work was supported in part by the JSPS Japan–US Cooperation Science Program (Pricipal Investigators: K. Shibata and K. I. Nishikawa).

References

Athay, R. G., & Moreton, G. E. 1961, ApJ, 133, 935
Brueckner, G. E., Howard, R. A., Koomen, M. J., Korendyke, C. M., Michels, D. J., Moses, J. D., Socker, D. G., Dere, K. P., et al. 1995, Sol. Phys., 162, 357
Delaboudinière, J.-P., Artzner, G. E., Brunaud, J., Gabriel, A. H., Hochedez, J. F., Millier, F., Song, X. Y., Au, B., et al. 1995, Sol. Phys., 162, 291
Kai, K. 1970, Sol. Phys., 11, 310
Klassen, A., Aurass, H., Mann, G., & Thompson, B. J. 2000, A&A, 141, 357
Kondo, T., Isobe, T., Igi, S., Watari, S., & Tokumaru, M. 1995, J. Commun. Res. Lab., 42, 111
Kurokawa, H., Ishiura, K., Kimura, G., Nakai, Y., Kitai, R., Funakoshi, Y., & Shinkawa, T. 1995, J. Geomag, Geoelectr., 47, 1043
Mann, G., Jansen, F., MacDowall, R. J., Kaiser, M. L., & Stone, R. G. 1999, A&A, 348, 614
Moreton, G. E. 1960, AJ, 65, 494
Moreton, G. E. 1961, Sky and Telescope, 21, 145
Moreton, G. E., & Ramsey, H. E. 1960, PASP, 72, 357
Moses, D., Clette, F., Delaboudinière, J.-P., Artzner, G. E., Bougnet, M., Brunaud, J., Carabetian, C., Gabriel, A. H., et al. 1997, Sol. Phys., 175, 571
Scherrer, P. H., Bogart, R. S., Bush, R. I., Hoeksema, J. T., Kosovichev, A. G., Schou, J., Rosenberg, W., Springer, L., et al. 1995, Sol. Phys., 162, 129
Smith, S. F., & Harvey, K. L. 1971, in Physics of the Solar Corona, ed. C. J. Macris (Dordrecht: Reidel), 156
Thompson, B. J., Gurman, J. B., Neupert, W. M., Newmark, J. S., Delaboudinière, J.-P., St. Cyr, O. C., Stezelberger, S., Dere, K. P., Howard, R. A., & Michels, D. J. 1999, ApJ, 517, 151
Thompson, B. J., Plunkett, S. P., Gurman, J. B., Newmark, J. S., St. Cyr, O. C., & Michels, D. J. 1998, Geophys. Res. Lett., 25, 2465
Thompson, B. J., Reynolds, B., Aurass, H., Gopalswamy, N., Gurman, J. B., Hudson, H. S., Martin, S. F., & St. Cyr, O. C. 2000, Sol. Phys., 193, 161
Uchida, Y. 1968, Sol. Phys., 4, 30
Uchida, Y. 1970, PASJ, 22, 341
Uchida, Y. 1974, Sol. Phys., 39, 431
Uchida, Y., Tanaka, T., Hata, M., & Cameron, R. 2001, Publ. Astron. Soc. Australia, 18, 345
Wang, T., Yan, Y., Wang, J., Kurokawa, H., & Shibata, K. 2002, ApJ, in press
Wang, Y.-M. 2000, ApJ, 543, L89
Warmuth, A., Vrsnak, B., Aurass, H., & Hanslmeier, A. 2001, ApJ, 560, L105
Yan, Y., Yu, Q., & Kang, F. 1991, Sol. Phys., 136, 195
Yan, Y., Yu, Q., & Shi, H. 1993, in Advances in Boundary Element Techniques, ed. J. H. Kane, G. Maier, N. Tosaka, & S. N. Atluri (New York: Springer-Verlag), 447